The College of Engineering
University of Wisconsin-Madison

Wisconsin Electric Machines and Power Electronics Consortium

RESEARCH REPORT
87-14

An Extended Kalman Filter Approach to Rotor Time Constant Measurement in PWM Induction Motor Drives

L. C. Zai and T. A. Lipo
Department of Electrical and Computer Engineering
University of Wisconsin-Madison
1415 Johnson Drive
Madison, WI 53706-1691

WEMPEC

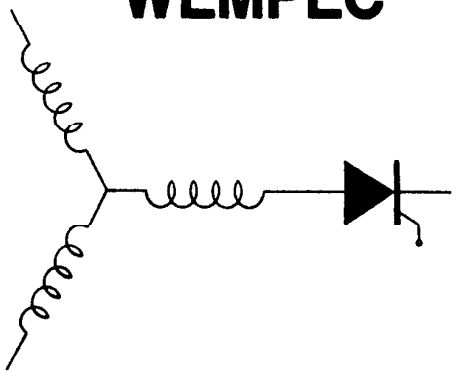

Department of Electrical and Computer Engineering
1415 Johnson Drive
Madison, Wisconsin 53706

July 1987

AN EXTENDED KALMAN FILTER APPROACH TO ROTOR TIME CONSTANT MEASUREMENT IN PWM INDUCTION MOTOR DRIVES

L.C. Zai and T.A. Lipo
University of Wisconsin
Department of Electrical and Computer Engineering
1415 Johnson Drive
Madison, WI 53706

Abstract - A rotor time constant estimation technique for the purpose of updating the control gains of an induction motor field orientation controller is described. An extended Kalman filter is employed to estimate the inverse rotor time constant on-line by only using measurements of the stator voltages and currents, and rotor speed of an induction motor. The motor is driven by a pulse width modulated (PWM) inverter with or without current feedback loops. By utilizing the wideband harmonic content inherent in conventional PWM voltage waveforms, no external random noise test signal is required for parameter estimation. Both simulation and experimental results demonstrate that the filter is capable of estimating the rotor time constant while the rotor speed is either constant or varying.

Introduction

Field orientation techniques utilizing microprocessors are now in widespread use for the control of induction motor drives in high performance applications. In general, two generic types of field-oriented control schemes are available. The first scheme, originally devised by Hasse [1], is an indirect flux sensing method wherein the rotor flux is estimated from the real-time machine model, stator current and voltage vectors, and rotor speed. This estimate is then fed forward to the flux and torque controller. The second scheme, developed by Blaschke [2], employs direct sensing of the air gap flux vector by use of Hall Effect sensors, search coils or other measurement techniques. The measured air gap flux is fed back to a controller enabling rotor flux to be regulated directly. The indirect scheme, by virtue of its simpler sensing arrangement, is the favored method in industry today. However, its performance strongly depends on the motor parameters, particularly the rotor time constant.

Recent work [3,4] on the influence of motor parameter deviations on indirect field orientation control systems indicates that error in the rotor time constant results in steady state operation with incorrect values of torque and flux. Also, the transient torque exhibits an oscillatory response and can not follow rapid changes in the torque command. Numerous methods [5-10] have been proposed to circumvent this problem. However, all of these methods identify the rotor time constant by injecting test signals into the motor which disturbs the normal operating functions of the drive.

In general, the field-oriented control principle can be applied without regard to the type of inverter. However, the recent activity in the development of high-power bipolar transistors has made the current-regulated pulse width modulated (CRPWM) inverter the popular choice in fast response ac servo applications [11,12]. This approach employs a fast-switching PWM inverter to control the currents supplied to the motor on an almost instantaneous basis. It is demonstrated in this paper that the resulting spectrum of the PWM voltages spreads over a very broad band of frequency. This wideband harmonic spectrum can be considered as a noise input to the drive which is impressed on the motor by the inverter itself. Hence, a random input for parameter identification is inherently available and no external test signals are required for the machine parameter estimation. When the motor speed changes, the machine model becomes, in effect, a two input/two output time varying system with a superimposed noise input. The extended Kalman filter approached is ideally suited to parameter estimation of such a system. In this paper it is demonstrated that parameter identification by means of an extended Kalman filter appears to be a viable, computationally efficient candidate for the on-line estimation of the rotor time constant.

Influence of Rotor Time Constant Change on Indirect Field Orientation Control Performance

The principle of field orientation is thoroughly presented in reference [12]. The dynamic behavior of a three-phase and three-wire induction machine with a squirrel-cage rotor can be described in a d-q rotating reference frame. With proper constraints, the d-q frame can be made to rotate synchronously with the stator or rotor flux. The so-called field oriented control is to allow the rotor flux entirely aligned with the d-axis of the d-q frame.

With a CRPWM inverter, the output currents and the frequency are the controllable variables. Indirect field orientated control can be considered as a special means for controlling the stator currents and slip frequency of an induction machine. By properly selecting the command stator currents i_{qs}^{e*} and i_{ds}^{e*}, the rotor flux can be placed in the d-axis provided that the slip angular frequency ω_s can follow the constraint,

$$\omega_s = \frac{r_r}{L_r} \frac{L_m i_{qs}^e}{\lambda_{dr}^e} \tag{1}$$

where the rotor flux linkage λ_{dr}^e is defined by

$$(1 + \frac{L_r}{r_r} p)\, \lambda_{dr}^e = L_m i_{ds}^e \tag{2}$$

where $p = d/dt$.

Equation 2 implies that in the steady-state,

$$\lambda_{dr}^e = L_m i_{ds}^e \quad \text{(steady state)} \tag{3}$$

The output torque of the motor is

$$T = \frac{3}{2} \frac{P}{2} (\frac{L_m}{L_r}) \lambda_{dr}^e i_{qs}^e \tag{4}$$

where the i_{qs}^e, i_{ds}^e and λ_{dr}^e are defined in the synchronous reference frame. The torque and flux can thus be independently controlled by i_{qs}^e and i_{ds}^e respectively. Since the stator current commands to the CRPWM inverter are preselected, the necessary stator frequency command can be obtained by simply summing the command slip frequency with the measured rotor frequency (i.e. speed).

$$\omega_e^* = \omega_r + \omega_s^* \tag{5}$$

For an indirect field orientated controller, the command slip frequency ω_s^* is determined by substituting a nominal inverse rotor time constant r_r^*/L_r^* in Eq. 1, and the slip angular frequency command ω_s^* becomes

$$\omega_s^* = \left[\frac{r_r}{L_r}\right]^* \frac{L_m i_{qs}^{e*}}{\lambda_{dr}^{e*}} \tag{6}$$

Asterisks are used to denoted the command or input quantities. If the value of inverse rotor time constant used in the Eq. 6 deviates from the real value, decoupling control of the flux and the torque will be lost. Accordingly, the steady state and the transient responses of the indirect field orientated drive system will be degraded. This phenomenon is referred to as "detuning" of the controller. In the steady state, detuning can result in the machine being either overexcited or underexcited. Overexciting a machine can cause it to saturate and thus increase the losses of the machine. On the other hand, a machine is not being efficiently used if it is underexcited. Furthermore, the transient output torque of the machine exhibits an oscillatory response and can not follow a step change in the input torque command. Computer simulation of the detuning effects due to variations of the inverse rotor time constant is shown in Fig. 1.

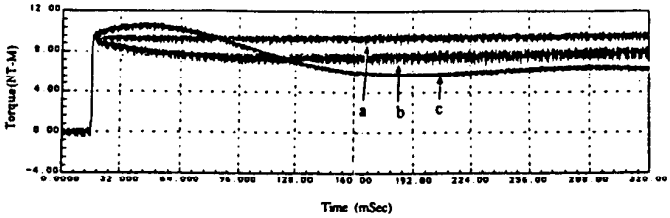

Fig. 1 Torque Response of a 3-hp Induction Machine Driven by a CRPWM Inverter with Indirect Field Orientation Control. (a) $(r_r/L_r)^* = r_r/L_r$, (b) $(r_r/L_r)^* = 0.5r_r/L_r$ (c) $(r_r/L_r)^* = 1.5r_r/L_r$.

Extended Kalman Filter Algorithm

The extended Kalman filter can be summarized as follows [13]. Let the system of interest be described by the dynamic model

$$\dot{\mathbf{x}}(t) = \mathbf{f}[\mathbf{x}(t),\mathbf{u}(t),t] + \mathbf{G}(t)\mathbf{w}(t) \tag{7}$$

where $\mathbf{x}(t_0)$ is described as the initial condition with mean $\mathbf{x}_0$ and covariance $\mathbf{P}_0$ and $\mathbf{u}(t)$ is the deterministic input, and $\mathbf{w}(t)$ is a zero mean white Gaussian noise that is independent of $\mathbf{x}(t_0)$, with covariance $\mathbf{Q}(t)$. Let the available discrete time measurements be modeled as

$$\mathbf{z}(t_i) = \mathbf{h}[\mathbf{x}(t_i),t_i] + \mathbf{v}(t_i) \tag{8}$$

where $\mathbf{v}(t_i)$ is a zero-mean white Gaussian noise that is independent of $\mathbf{x}(t_0)$ and $\mathbf{w}(t)$, with covariance $\mathbf{R}(t_i)$.

The extended Kalman filter measurement update incorporates the measurement $\mathbf{z}(t_i)$ by means of

$$\mathbf{K}(t_i) = \mathbf{P}(t_i^-)\mathbf{H}^T[\hat{\mathbf{x}}(t_i^-),t_i]\left\{\mathbf{H}[\hat{\mathbf{x}}(t_i^-),t_i]\mathbf{P}(t_i)\mathbf{H}^T[\hat{\mathbf{x}}(t_i^-),t_i] + \mathbf{R}(t_i)\right\}^{-1} \tag{9}$$

$$\hat{\mathbf{x}}(t_i^+) = \hat{\mathbf{x}}(t_i^-) + \mathbf{K}(t_i)\left\{\mathbf{z}(t_i - \mathbf{h}[\hat{\mathbf{x}}(t_i^-),t_i]\right\} \tag{10}$$

$$\mathbf{P}(t_i^+) = \mathbf{P}(t_i^-) - \mathbf{K}(t_i)\mathbf{H}[\hat{\mathbf{x}}(t_i^-),t_i]\mathbf{P}(t_i^-) \tag{11}$$

$$= \left\{\mathbf{I} - \mathbf{K}(t_i)\mathbf{H}[\hat{\mathbf{x}}(t_i^-),t_i]\right\}\mathbf{P}(t_i^-)\left\{\mathbf{I} - \mathbf{K}(t_i)\mathbf{H}[\hat{\mathbf{x}}(t_i^-),t_i]\right\}^T$$

$$+ \mathbf{K}(t_i)\mathbf{R}(t_i)\mathbf{K}^T(t_i) \tag{12}$$

where H is defined as the m-by-n partial derivative matrix :

$$\mathbf{H}[\hat{\mathbf{x}}(t_i^-),t_i] = \left.\frac{\partial \mathbf{h}[\mathbf{x},t_i]}{\partial \mathbf{x}}\right|_{\mathbf{x}=\hat{\mathbf{x}}(t_i^-)} \tag{13}$$

An estimate of $\mathbf{x}(t)$ is propagated from t_i to t_{i+1} by integrating

$$\dot{\hat{\mathbf{x}}}(t/t_i) = \mathbf{f}[\hat{\mathbf{x}}(t/t_i),\mathbf{u}(t),t] \tag{14}$$

$$\dot{\mathbf{P}}(t/t_i) = \mathbf{F}[\hat{\mathbf{x}}(t/t_i),t]\mathbf{P}(t/t_i) + \mathbf{P}(t/t_i)\mathbf{F}^T[\hat{\mathbf{x}}(t/t_i),t] + \mathbf{G}(t)\mathbf{Q}(t)\mathbf{G}^T(t) \tag{15}$$

where $\mathbf{x}(t/t_i)$ denotes the solution to Eq. 14, but starting from the initial condition of $\hat{\mathbf{x}}(t_i^+)$, i.e., the solution over the interval $[t,t_{i+1}]$. The $\mathbf{P}(t/t_i)$ is defined in the same manner. Hence, the initial conditions of the above two equations are

$$\hat{\mathbf{x}}(t_i/t_i) = \hat{\mathbf{x}}(t_i) \tag{16}$$

$$\mathbf{P}(t_i/t_i) = \mathbf{P}(t_i^+) \tag{17}$$

However, for the first time interval (from t_0 to t_1), the initial conditions would be $\mathbf{x}_0$ and $\mathbf{P}_0$. In Eq. 15, F is the n-by-n partial derivative matrix :

$$\mathbf{F}[\hat{\mathbf{x}}(t/t_i),t_i] = \left.\frac{\partial \mathbf{f}[\mathbf{x},\mathbf{u}(t),t]}{\partial \mathbf{x}}\right|_{\mathbf{x}=\hat{\mathbf{x}}(t/t_i)} \tag{18}$$

during the entire time interval $[t_i, t_{i+1})$. Upon integrating Eq. 14 and Eq. 15 to the next sampling time t_{i+1}, the $\hat{\mathbf{x}}(t_{i+1}/t_i)$ and $\mathbf{P}(t_{i+1}/t_i)$ are generated. They are used for the next measurement update,

$$\hat{\mathbf{x}}(t_{i+1}^-) = \hat{\mathbf{x}}(t_{i+1}/t_i) \tag{19}$$

$$\mathbf{P}(t_{i+1}^-) = \mathbf{P}(t_{i+1}/t_i) \tag{20}$$

Note that F, H, K, and P are evaluated with the most recent estimate generated by the filter itself. In contrast to the conventional and linearized Kalman filters, the equations for propagating and updating the estimation error covariance matrix P are based on the new state estimate. Therefore the covariance and gain matrices can not be precomputed without knowing the state estimates and the actual measurements.

Estimation of the Inverse Rotor Time Constant with an Extended Kalman Filter

A general form of a current-regulated PWM drive with data-acquisition circuits and an extended Kalman filter is shown in Fig. 2. A proportional- plus-integral compensator is usually employed as the current compensator. The voltage isolator in Fig. 2 is to prevent the data-acquisition circuits and the microprocessor, an IBM PC-AT, from being damaged by the high voltage of the PWM drive. Three integrators are used to recover the fundamental components of the voltage signals. A high precision speed measurement is achieved by using a speed measurement circuit [13].

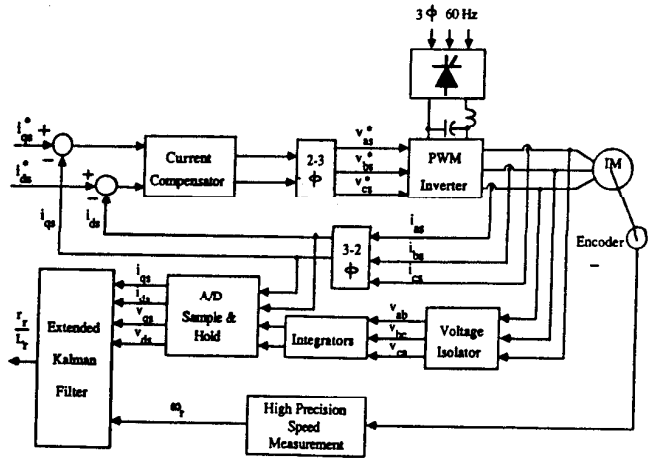

Fig. 2 On-Line Estimation of the Inverse Rotor Time Constant of an Induction Machine.

For simplicity, all the variables in the following part of this paper are defined in the stationary reference frame. The system should be modeled in the form of a vector set of differential equations in order that a Kalman filter can be applied to the system. Utilizing an induction motor model in the stationary reference frame, let the state variables be defined as,

$$\begin{bmatrix} x_1(t) \\ x_2(t) \\ x_3(t) \\ x_4(t) \\ x_5(t) \end{bmatrix} = \begin{bmatrix} i^s_{qs}(t) \\ i^s_{ds}(t) \\ i^s_{qr}(t) \\ i^s_{dr}(t) \\ \dfrac{r_r}{L_r}(t) \end{bmatrix} \tag{21}$$

The spectrum of a typical PWM voltage, shown in Fig. 3, indicates that one fundamental component and wideband harmonics are contained in this voltage. After assuming the fundamental component of a voltage signal as the deterministic input and all the wideband harmonics as white Gaussian noises, the dynamic behavior of a three phase induction machine can be modeled as

$$\dot{\mathbf{x}}(t) = \mathbf{f}[\mathbf{x}(t),\mathbf{u}(t),t] + \mathbf{G}(t)\mathbf{W}(t) \tag{22}$$

where,

$$\mathbf{f}[\mathbf{x}(t),\mathbf{u}(t),t] = [f_1(t),f_2(t),f_3(t),f_4(t),f_5(t)]^T =$$

$$\frac{L_s L_r}{L_s L_r - L_m^2} \begin{bmatrix} -\dfrac{r_s}{L_s}x_1 - \dfrac{L_m^2}{L_s L_r}\omega_r x_2 + \dfrac{L_m}{L_s}x_3 x_5 - \dfrac{L_m}{L_s}\omega_r x_4 + \dfrac{1}{L_s}v^s_{qsf} \\ \dfrac{L_m^2}{L_s L_r}\omega_r x_1 - \dfrac{r_s}{L_s}x_2 + \dfrac{L_m}{L_s}\omega_r x_3 + \dfrac{L_m}{L_s}x_4 x_5 + \dfrac{1}{L_s}v^s_{dsf} \\ \dfrac{L_m}{L_r}\dfrac{r_s}{L_s}x_1 + \dfrac{L_m}{L_r}\omega_r x_2 - x_3 x_5 + \omega_r x_4 - \dfrac{1}{L_s}\dfrac{L_m}{L_r}v^s_{qsf} \\ \dfrac{-L_m}{L_r}\omega_r x_1 + \dfrac{L_m}{L_r}\dfrac{r_s}{L_s}x_2 - \omega_r x_3 - x_4 x_5 - \dfrac{1}{L_s}\dfrac{L_m}{L_r}v^s_{dsf} \end{bmatrix} \tag{23}$$

$$\mathbf{G}(t) = \frac{L_s L_r}{L_s L_r - L_m^2} \begin{bmatrix} \dfrac{1}{L_s} & 0 & 0 \\ 0 & \dfrac{1}{L_s} & 0 \\ -\dfrac{1}{L_s}\dfrac{L_m}{L_r} & 0 & 0 \\ 0 & -\dfrac{1}{L_s}\dfrac{L_m}{L_r} & 0 \\ 0 & 0 & 1 \end{bmatrix} \tag{24}$$

$$\mathbf{w}(t) = \begin{bmatrix} w_1(t) \\ w_2(t) \\ n(t) \end{bmatrix} \tag{25}$$

where v_{qsf} and v_{dsf} are the fundamental components of PWM voltage signals, and the $w_1(t)$ and $w_2(t)$ are the wideband harmonics. Due to the fact that PWM voltage signals are high frequency square waves, it is not practical to acquire the voltage signals by direct A/D conversion because of the aliasing problem. Since normal filters can introduce phase shift, they are also ruled out as the prefilters before the sample-and-hold devices. However, in a $d-q$ coordinate system, it is well known that the voltage v_{ds} leads v_{qs} by 90°. An integrator is also known to introduce

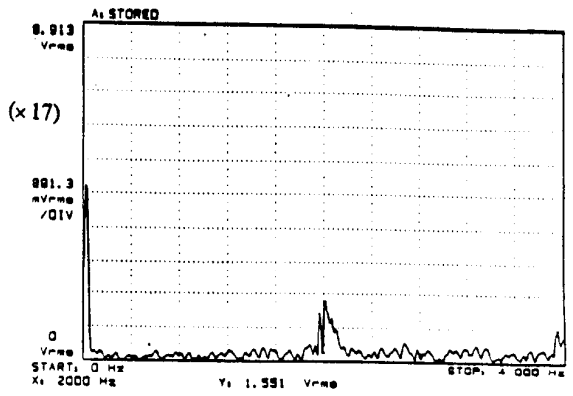

Fig. 3 Experimental Voltage Spectrum of a CRPWM Inverter.

a 90° phase lag and also to attenuate high frequency signals. Hence the following equations can be used to separate the fundamental voltage components of the PWM inverter, v_{qs} and v_{ds}, from the high frequency harmonics.

$$v_{qsf} = \omega_e \int v_{ds}\, dt \tag{26}$$

$$v_{dsf} = \omega_e \int -v_{qs}\, dt \tag{27}$$

The experimental results of the recovered fundamental signals are illustrated in Fig. 4. By using integrators as the prefilters it is important to observe that the performance of the extended filter in transient conditions is limited. This means the stator frequency needs to be kept at a constant value or is only allowed to change very slowly during the estimation process. If other filtering techniques can be developed to remove this constraint, the ability of the filter could be greatly enhanced.

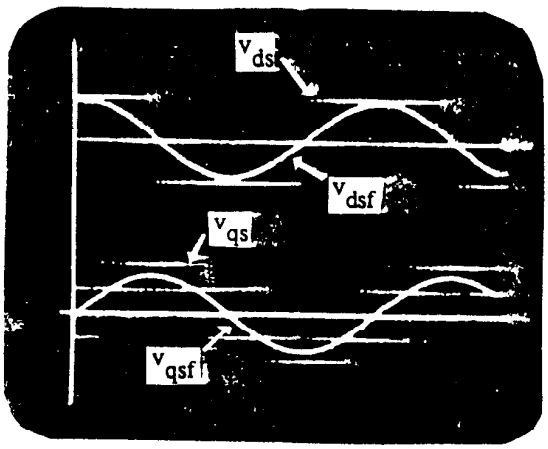

Fig. 4 Experimentally Recovered Fundamental Components of Stator Voltages.

The discrete-time measurement model can be written as

$$\mathbf{z}(t_i) = \mathbf{h}[\mathbf{x}(t_i),t_i] + \mathbf{v}(t_i) \tag{28}$$

where,

$$\mathbf{z}(t_i) = \begin{bmatrix} i^s_{qs}(t_i) \\ i^s_{ds}(t_i) \end{bmatrix} \tag{29}$$

$$\mathbf{h}[x(t_i),t_i] = \begin{bmatrix} i^s_{qs}(t_i) \\ i^s_{ds}(t_i) \end{bmatrix} \tag{30}$$

Assume now that $v(t_i)$ is a white Gaussian noise vector, which includes the wideband harmonics in the motor currents as well as measurement noise of the current sensors. From Eq. 23 and Eq. 30 the quantities F and H can be defined as

$$\mathbf{F}[\mathbf{x}(t/t_i),t] = \left.\frac{\partial \mathbf{f}[\mathbf{x}(t),\mathbf{u}(t),t]}{\partial \mathbf{x}}\right|_{\mathbf{x}=\hat{\mathbf{x}}(t/t_i)} \tag{31}$$

or

$$\mathbf{F} = \frac{L_s L_r}{L_s L_r - L_m^2}\begin{bmatrix} -\frac{r_s}{L_s} & -\frac{L_m^2}{L_s L_r}\omega_r & \frac{L_m}{L_s}x_5 & -\frac{L_m}{L_s}\omega_r & \frac{L_m}{L_s}x_3 \\ \frac{L_m^2}{L_s L_r}\omega_r & -\frac{r_s}{L_s} & \frac{L_m}{L_s}\omega_r & \frac{L_m}{L_s}x_5 & \frac{L_m}{L_s}x_4 \\ L_m L_r \frac{r_s}{L_s} & \frac{L_m}{L_r}\omega_r & -x_5 & \omega_r & -x_3 \\ -\frac{L_m}{L_r}\omega_r & \frac{L_m}{L_r}\frac{r_s}{L_s} & -\omega_r & -x_5 & -x_4 \\ 0 & 0 & 0 & 0 & 0 \end{bmatrix}$$

$$\mathbf{H}[\mathbf{x}(t/t_i),t] = \left.\frac{\partial \mathbf{h}[\mathbf{x}(t),\mathbf{u}(t),t]}{\partial x}\right|_{\mathbf{x}=\hat{\mathbf{x}}(t/t_i)} \tag{32}$$

$$\mathbf{H}[\mathbf{x}(t_i),t] = \begin{bmatrix} 1 & 0 & 0 & 0 & 0 \\ 0 & 1 & 0 & 0 & 0 \end{bmatrix}$$

Simulation and Experimental Results

Both digital computer simulations and laboratory experiments have been carried out to verify the feasibility of estimating the inverse rotor time constant with an extended Kalman filter. The results from experiments agree with those from simulations. Two different types of PWM drives and one 3-hp squirrel-cage induction motor were used in the experiments. One of the drives has a current feedback loop (CRPWM), while the other inverter is without current feedback loops (PWM).

Two methods were used to examine the accuracy of the estimation results. One is the "absolute comparison" that is to compare the estimated r_r/L_R with the value calculated from the manufacturer's specifications and measurements. The other test is "relative comparison"; that is to operate a motor in a same test condition except at different temperatures. The change of estimates is compared with the change of temperatures. The "absolute comparison" can be affected by the accuracy of laboratory instruments and transducers, but the "relative comparison" is less sensitive to measurement errors. One assumption made in these comparisons was that the stator and rotor of a induction machine were at the same temperature. As a result, the rotor resistance can be assumed to vary linearly in proportion to its stator resistance, and from the measurement of the stator resistance, the rotor resistance can be computed as

$$r_r(T_2) = r_r(T_1)\,\frac{r_s(T_2)}{r_s(T_1)} \tag{33}$$

In the above equation, $r_r(T_1)$ and $r_s(T_1)$ are the rotor resistance and stator resistance at temperature T_1, whereas $r_r(T_2)$ and $r_s(T_2)$ are at temperature T_2. The $r_r(T_1)$ and $r_s(T_1)$ can be obtained from the manufacture data. If $r_s(T_2)$ is measured at a certain temperature, the $r_r(T_2)$ is also known.

The experimental results for a PWM inverter manufacturered by Allen-Bradley together with the simulation results, are summarized in Table 1, and the results for a CRPWM drive are listed in Table 2. All the estimates are close to the values from calculation. The change in estimates shows good agreement with the change in temperatures, indicated by the change in the stator resistance. The current waveform of a PWM inverter is shown in Fig. 5. Fig. 6 illustrates the estimates of the r_r/L_r at two different temperatures, which clearly shows that the estimated r_r/L_r increases when the motor becomes hot.

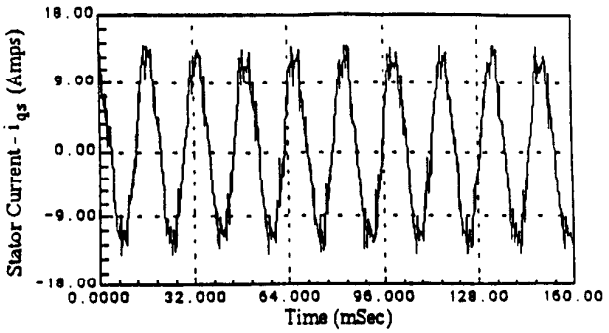

Fig. 5 Experimental Stator Current i_{qs} of a 3-hp Induction Machine Driven by a PWM Inverter.

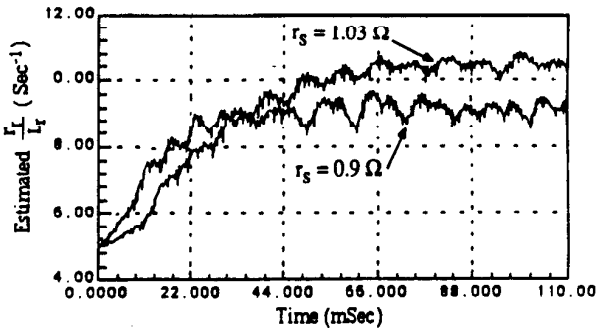

Fig. 6 Experimental Estimates of r_r/L_r at Two Different Temperatures.

Under practical conditions, it is very difficult to keep the rotor speed constant such that the estimation can be done. One experiment was designed to examine the performance of the filter while the rotor speed is varying. A CRPWM was used to perform the experiment. First, the motor was allowed to rotate at a constant speed of 500 rpm. Subsequently, a large load torque was applied to the rotor shaft, which tended to stall the motor. Since the stator current and frequency (Fig. 7) were held constant, the stator voltage (Fig. 8) decreases according to the decrease in the rotor speed (Fig. 9). This result occurs because the impedance of the machine becomes smaller when the slip is increased. Figure 10 depicts the estimated inverse rotor time constant r_r/L_r, which demonstrates that the filter can still properly function. The above experimental results show that the extended Kalman filter can effectively estimate the r_r/L_r over a wide speed range from 1727 rpm to 115 rpm.

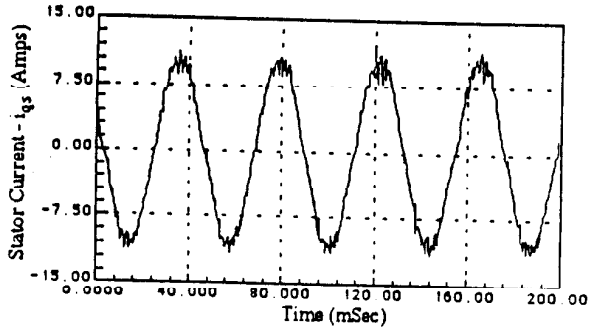

Fig. 7 Experimental Stator Current i_{qs} of a 3-hp Induction Machine Driven by a CRPWM Inverter.

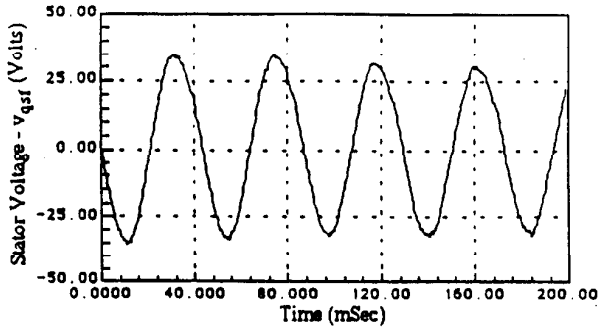

Fig. 8 Experimental Stator Voltage v_{qs} for Varying Rotor Speed.

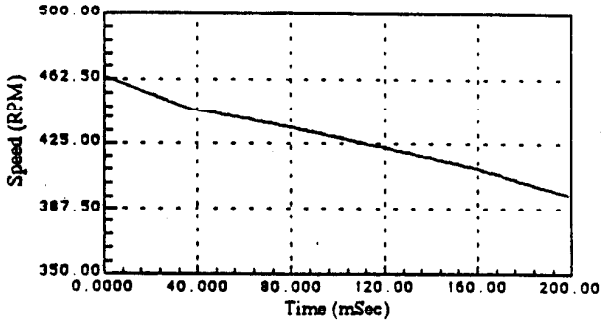

Fig. 9 Experimental Rotor Speed for Varying Load.

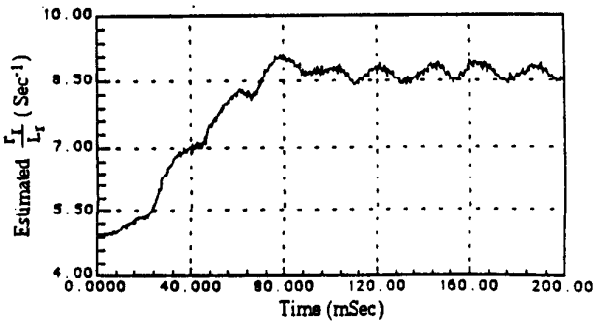

Fig. 10 Estimate of r_r/L_r During a Varying Rotor Speed Condition.

On-Line Calculation of Magnetizing Inductance

When the parameters used in the filter model are not the same as the real machine parameters, some variations of the estimated r_r/L_r can be found. However, from the experiments, it was noted that only variations in magnetizing inductance L_m can introduce a significant error in the estimate. Therefore, a precise knowledge of L_m becomes important. Conventionally, a saturation curve and the air gap emf are used to find the magnetizing inductance through a look-up-table. The air gap emf is motor terminal voltage minus the voltage drop across stator resistance and leakage inductance. This method inherently has a certain inaccuracy because the magnetizing inductance is mainly dominated by the magnetizing current, but the air gap emf is a function of both the magnetizing inductance L_m and current i_m. For instance, either a small L_m and a large i_m or a large L_m and a small i_m may produce the same air gap emf.

An alternative for determining L_m is to deal with the magnetizing current i_m directly. A new L_m-versus-i_m saturation curve can be constructed from the no load test, shown in Fig. 11. The remaining problem to be solved is to find the magnetizing current during normal machine operation when the rotor current is no longer zero and not perfectly known. Figure 12 illustrates the phase angle θ_s between the stator voltage and current for a rated load condition. A phasor diagram representing the equivalent circuit of an induction motor is shown in Fig. 13. The phase angle θ_s can be used to calculate the magnetizing current I_m with the following equations.

$$\tilde{E} = \tilde{V} - \tilde{I}_s\,(r_s + jX_{ls}) \tag{34}$$

$$E = [V - (I_s r_s \cos\theta_s + I_s X_{ls}\sin\theta_s)] - j(I_s X_{ls}\cos\theta_s - I_s r_s \sin\theta_s) \tag{35}$$

$$\theta_e = \tan^{-1}\frac{I_s X_{ls}\cos\theta_s - I_s r_s \sin\theta_s}{V-(I_s r_s \cos\theta_s + I_s X_{ls}\sin\theta_s)} \tag{36}$$

$$\theta_r = \tan^{-1}\frac{X_{ls}}{(r_r/S)} \tag{37}$$

$$\tilde{I}_r = \frac{\tilde{E}}{r_r/S + jX_{lr}} \tag{38}$$

$$I_m = I_s\sin(\theta_s-\theta_e) - I_r\sin\theta_r \tag{39}$$

where

$$\tilde{V} = V\angle 0 \qquad \tilde{E} = E\angle -\theta_e$$
$$\tilde{I} = I_s\angle -\theta_s \qquad \tilde{I}_r = I_r\angle -\theta_r$$
$$\tilde{I}_m = I_m\angle -\theta_m$$

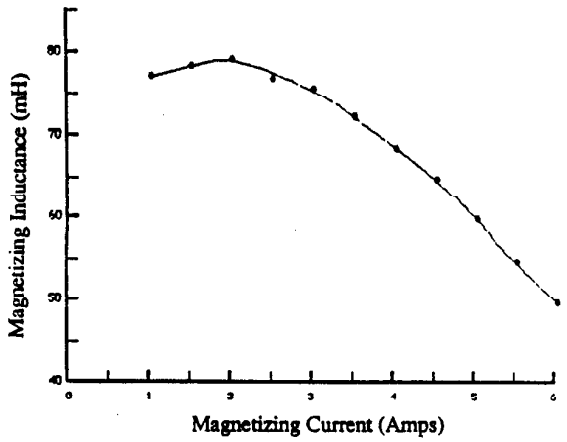

Fig. 11 L_m - vs - I_m Saturation Curve of a 3-hp Induction Machine.

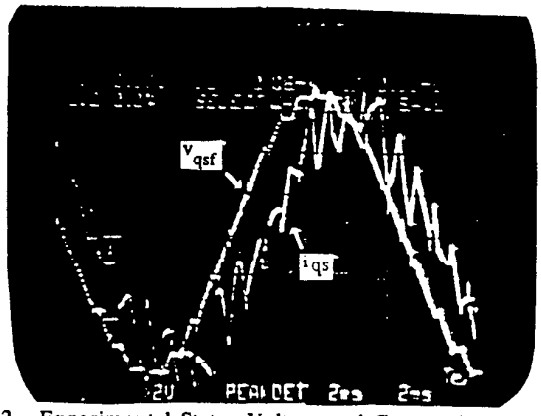

Fig. 12 Experimental Stator Voltage and Current in Rated Load Condition.

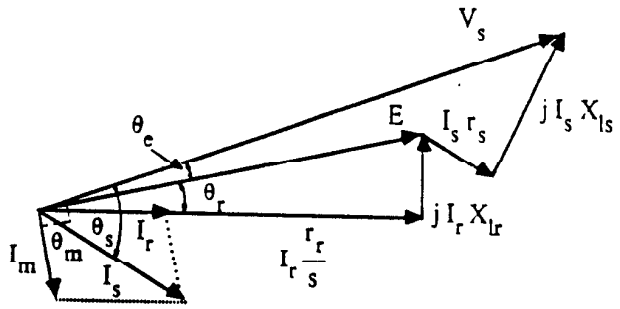

Fig. 13 Phasor Diagram Illustrating the Computation of Magnetizing Current.

In the above equations, X_{ls}, X_{lr}, and r_r are not exactly known. However, θ_e and θ_r are usually very small, and hence the effects of parameter variations can be reduced. The θ_s is the phase angle between the stator voltage and current, which can be computed by applying the Fast Fourier transform (FFT) to the voltage and current signals.

Conclusions

Field orientated control induction motor drive systems are presently considered as viable alternatives for replacing dc motor drives. However, changes in the rotor time constant have an important effect on the performance of the indirect field orientation drive system. An on-line technique for establishing the exact value of the rotor time constant of the induction motor without the use of additional sensors has been described. This technique has been verified by computer simulation and tested on two different types of inverters (PWM and CRPWM). Both simulation and experimental results demonstrate an extended Kalman filter can be used to accurately estimate the inverse rotor time constant when an induction motor operates under normal conditions. The approach should prove useful in high horsepower applications where rotor time constant changes can seriously deteriorate the performance of the drive.

References

1. K. Hasse, "On the Dynamics of Speed Control Static AC Drives with Squirrel-Cage Induction Machines," Ph.D. Dissertation, Technische Hochschule Darmstadt, 1969.
2. F. Blaschke, "Das Verfahren der Feldorientierung zur Regelung der Drehfeld- machine," ("The method of field orientation for control of three phase machines"), Ph.D. Dissertation, TU Braunschweig. 1974.
3. M. Koyama and H. Sugimoto, "Effects of Parameter Change on Coordinate Control System of Induction Motor," IPEC, Tokyo, 1983, pp. 684-695.
4. K. B. Nordin, D. W. Novotny and D. S. Zinger, "The Influence of Motor Parameter Deviations in Feedforward Field Orientation Drive Systems," IEEE-IAS Annual Meeting Conference Record, Sept. 30 - Oct. 4, 1984, pp. 525-531.
5. L. J. Garces, "Parameter Adaptation for the Speed-Controlled Static AC Drive with a Squirrel-Cage Induction Motor," IEEE-IAS Transactions, Vol. IA-16, No. 2, 1980, pp. 173-178.
6. T. Irisa, S. Takata, R. Ueda and T. Sonada, "On Reliability of Induction Machine for High Performance Based on Parameter Characteristics," IEEE-IAS Annual Meeting Conference Record, Oct. 3 - 7, 1983, pp. 547-554.
7. Hisao Kubota, Kouki Matsuse and Tadashi Fukao, "New Control Method of Inverter-Fed Induction Motor Drive by Using State Observer with Rotor Resistance Identification," Electrical Engineering in Japan, Vol. 105, No. 5, Sept. - Oct., 1985, pp. 119- 127.
8. Hidehiko Sugimoto and Shinzo Tamai, "Secondary Resistance Identification of an Induction Motor : Applied Model Reference Adaptive System and its Characteristics," IEEE-IAS Annual Meeting Conference Record, Oct. 6-11, 1985, pp. 613-620.
9. R. Gabriel and W. Leonhard, "Microprocessor Control of Induction Motor," IEEE-IAS International Semiconductor Power Converter Conference, May 24 - 27, 1982, pp. 385-396.
10. T. Matsuo and T. A. Lipo, "A Rotor Parameter Identification Scheme for Vector Controlled Induction Motor Drives," IEEE-IAS Annual Meeting Conference Record, Sept. 30 - Oct. 4, 1984, pp. 538-545.
11. Toshiaki Okuyama, Hiroshi Nagase and Yuzuru Kubota, "High Performance AC Motor Speed Control System Using GTO Converters," IPEC, Tokyo, 1983, pp. 720-730.
12. W. Leonhard,"Control of Electrical Drives", (book) Springer-Verlag, Berlin, 1985.
13 L.-C. Zai,"Application of an Extended Kalman Filter to Induction Machine Parameter Estimation", Ph.D. Thesis, Univ. of Wisconsin, 1986.
14 Peter S. Maybeck, "Stochastic Models, Estimation and Control," Vol. 1 and Vol. 2, Academic Press, 1982.

Drive	AB	AB	AB	AB	SIM	SIM
f_e (hz)	60.0	60.0	7.70	8.80	60.0	60.0
ω_r (rpm)	1727	1727	115	114	1727	1727
slip	0.0406	0.0406	0.502	0.568	0.0406	0.0406
Voltage (rms)	122.8	127.8	14.89	17.15	102.6	109.5
Current (rms)	8.72	8.15	7.71	8.00	6.98	7.00
r_s^{**} (ohm)	0.90	1.03	0.90	1.03	0.90 #	1.03 #
r_r^* (ohm)	0.586	0.670	0.586	0.670	0.586	0.670
L_m^* (mh)	65	65	78	78	65	65
L_r^* (mh)	66.8	66.8	79.8	79.8	66.8	66.8
$r_r / L_r^*(s^{-1})$	8.77	10.03	7.34	8.40	8.77	10.03
$r_r / L_r^{**}(s^{-1})$	9.2	10.4	8.1	9.1	8.2 #	9.4 #
% Change *	+ 14.37		+ 14.44		+ 14.37	
% Change **	+ 13.0		+ 12.4		+ 14.6 #	

* : from calculation.

** : from experiment.

: from simulation.

Table 1 Experimental and Simulation Results for PWM Inverter.

Drive	UW	UW	UW	UW	UW
f_e (hz)	23.54	23.54	6.10	6.10	23.18
ω_r (rpm)	658	643	121	132	395-462
slip	0.0683	0.0895	0.339	0.279	
Voltage (rms)	63.17	64.30	16.83	18.95	
Current (rms)	7.52	7.47	7.59	7.61	7.25
r_s^{**} (ohm)	0.94	1.06	0.94	1.05	0.94
r_r^* (ohm)	0.61	0.69	0.61	0.68	0.61
L_m^* (mh)	65	65	62	62	75
L_r^* (mh)	66.8	66.8	63.8	63.8	76.8
$r_r / L_r^*(s^{-1})$	9.16	10.33	9.59	10.71	7.97
$r_r / L_r^{**}(s^{-1})$	8.9	10.4	8.9	9.8	8.8
% Change *	+ 12.77		+ 11.70		
% Change **	+ 16.9		+ 10.1		

* : from calculation.

** : from experiment.

Table 2 Experimental Results for CRPWM Inverter.